Synthesis and Exfoliation of Quasi-1D (Zr,Ti)S₃ Solid Solutions for Device Measurements

Dmitry S. Muratov,¹* Vladislav O. Vanyushin,¹ Nataliia S. Vorobeva,² Polina Jukova,¹ Alexey Lipatov,² Evgeny A. Kolesnikov,¹ Dmitry Karpenkov,¹ Denis V. Kuznetsov,¹ Alexander Sinitskii^{2,3,*}

¹National University of Science and Technology "MISIS", Moscow 119991, Russia

²Department of Chemistry, University of Nebraska, Lincoln, NE 68588, United States

³Nebraska Center for Materials and Nanoscience, University of Nebraska, Lincoln, NE 68588, United States

*E-mails: <u>muratov@misis.ru</u> (Dmitry S. Muratov); <u>sinitskii@unl.edu</u> (Alexander Sinitskii)

KEYWORDS: quasi-one-dimensional materials, transition metal trichalcogenides, TiS₃, ZrS₃, solid solutions, mechanical exfoliation, field-effect transistors.

ABSTRACT

Transition metal trichalcogenides (TMTCs), such as TiS₃ and ZrS₃, attract growing interest because of their peculiar quasi-one-dimensional (quasi-1D) structure and promising electronic properties. In this study, we investigated $Zr_{1-x}Ti_xS_3$ solid solutions and demonstrated that they could be prepared through the direct reaction between Zr-Ti alloys and sulfur vapor at 800 °C. We varied the Zr/Ti atomic ratio in the alloys from 80/20 to 20/80 and found that in all cases the resulting solid solution crystals had a composition close to $Zr_{0.8}Ti_{0.2}S_3$. The excessive titanium, if present, formed the secondary TiS₂ phase, which was detected by the powder X-ray diffraction (XRD) analysis and observed in scanning electron microscopy (SEM) images in the form of hexagonal crystals. The $Zr_{1-x}Ti_xS_3$ solid solutions formed distinct needle-like crystals, whose shape was consistent with the quasi-1D structure of TMTCs. We demonstrated that these crystals could be mechanically exfoliated into thin nanoribbons by an adhesive tape approach and used for device fabrication and electrical measurements. The transport measurements of $Zr_{0.82}Ti_{0.18}S_{2.86}$ devices revealed their n-type conductivity and electron mobility of about 2 cm² V⁻¹ s⁻¹, as well as photoresponse to visible light.

1. Introduction

Transition metal trichalcogenides (TMTCs) with the MX₃ composition (M is a transition metal ion, such as Ti, Zr or Hf; X = S, Se or Te) are a family of quasi-one-dimensional (quasi-1D) materials with intriguing physical properties [1-3]. Within this family, titanium trisulfide (TiS₃) received most attention from researchers due to its promise for energy storage applications [4-6], theoretical predictions of high electron mobilities [7, 8] and thermoelectric properties [9, 10]. Similar to other TMTC materials, TiS₃ consists of covalently bonded 1D chains, which are assembled into crystals through weak van der Waals-like interactions [1-3]. TiS₃ crystals could be exfoliated using an adhesive tape into thin nanoribbons [11], which could be used for device fabrication and electrical measurements [12-14]. Previously, we reported that devices based on few-nm-thick TiS₃ nanoribbons show n-type behavior with field-effect mobilities up to 43 cm²V⁻¹s⁻¹ and on/off ratios >10³ [14], which makes them comparable to devices based on much more extensively studied transition metal dichalcogenides [15]. Transient absorption measurements of TiS₃ nanoribbons yielded a similar exciton mobility of about 50 cm²V⁻¹s⁻¹ [16].

While much less studied than TiS_3 , other members of the TMTC family offer a multitude of properties [2, 17] that could be utilized in various electronic devices and complement those of TiS_3 . For example, while TiS_3 has a band gap of about 1 eV [18-20], ZrS_3 has a larger band gap of about 2 eV [2, 17, 21] (correspondingly, TiS_3 crystals are black, while ZrS_3 crystals have a reddish color). The fact that TiS_3 and ZrS_3 are isostructural (Figure 1a) opens an opportunity of synthesizing $Zr_{1-x}Ti_xS_3$ solid solutions with a band gap tunable from near infrared to visible with x decreasing from 1 to 0, which could be relevant to a variety of electronic and optoelectronic applications, ranging from field-effect transistors (FETs) and photodetectors to memory devices and gas sensors.

Several previous studies focused on the solid solutions of TMTC materials. For example, Brattas and Kjekshus investigated ternary solid solutions in ZrS₃-ZrSe₃-ZrTe₃ and HfS₃-HfSe₃-HfTe₃ series and demonstrated that it is possible to tune the band gap by varying the chalcogen ratio in solid solutions like ZrS_{3-x}Se_x [2]. However, less attention has been paid to the TMTC solid solutions with variable transition metal composition, such as Zr_{1-x}Ti_xS₃ solid solutions [22-24], and no attempts to exfoliate such crystals and fabricate electronic devices, similar to the recent TiS₃ studies [12-14], have been reported.

In this study, we investigated the synthesis of Zr_{1-x}Ti_xS₃ crystals, their mechanical exfoliation and implementation in FET devices. As precursors for the synthesis of these solid solutions we propose to use Zr-Ti alloys, utilizing mutual solubility of titanium and zirconium in each other [25]. We synthesized a continuous series of Zr-Ti alloys by the arc-melting technique and used them in a direct reaction with sulfur vapor in vacuum sealed ampoules to grow Zr_{1-x}Ti_xS₃ crystals. The crystals were characterized by scanning electron microscopy (SEM), X-ray diffraction (XRD), energy-dispersive X-ray (EDX) spectroscopy, Raman spectroscopy, X-ray photoelectron spectroscopy (XPS) and used for device fabrication and electrical measurements.

2. Experimental

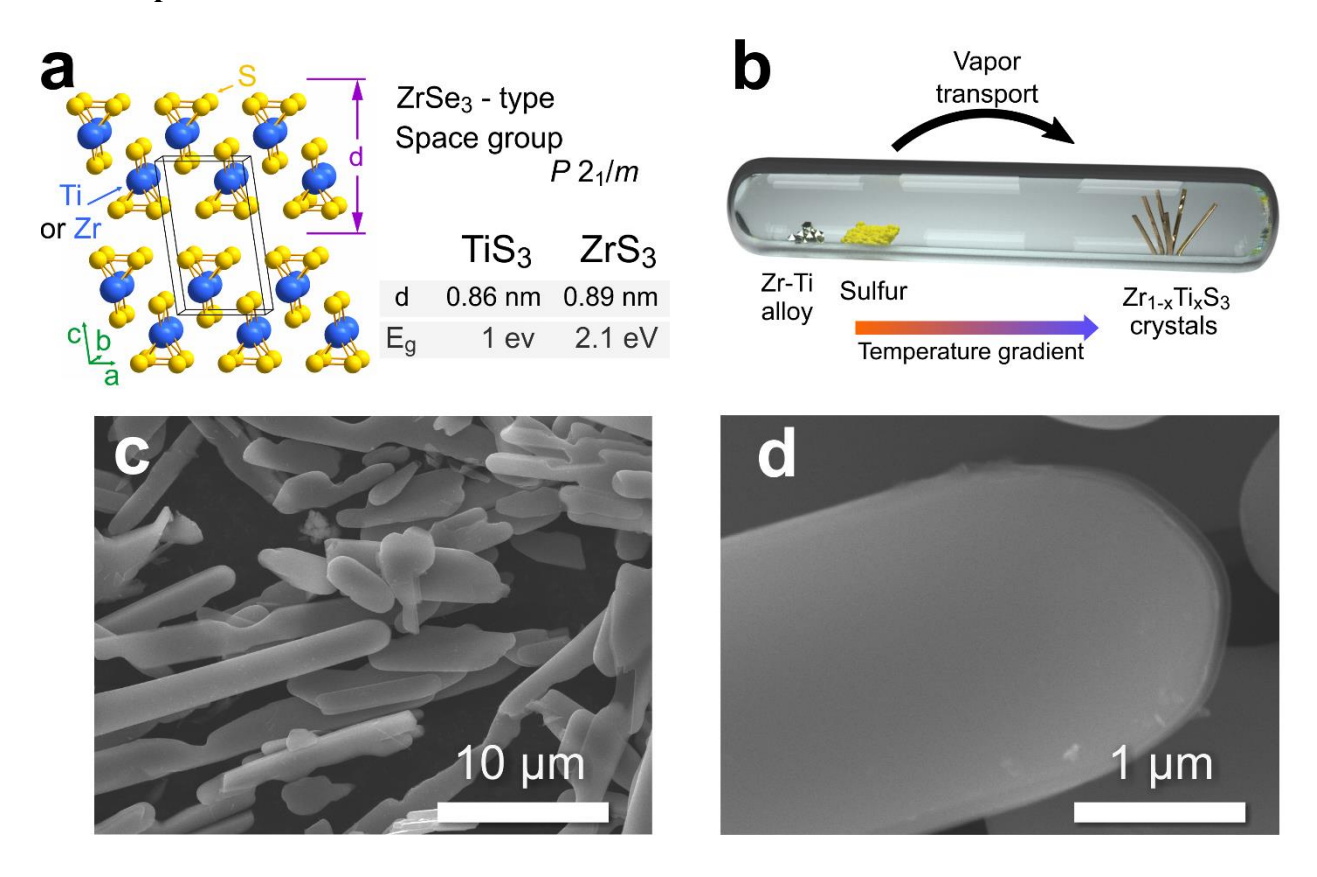


Figure 1. (a) Crystallographic data for TiS₃ and ZrS₃. (b) Scheme of the synthesis of Zr_{1-x}Ti_xS₃ crystals. (c,d) SEM images of the crystals grown from the Zr_{0.6}Ti_{0.4} alloy.

 $Zr_{1-x}Ti_x$ alloys were produced by co-melting pure Ti and Zr metals using a high-vacuum arc-melting furnace (Arcast Arc 200). Titanium and zirconium were mixed in 20/80, 40/60, 60/40 and 80/20 molar ratios, and the chemical compositions of the resulting $Zr_{1-x}Ti_x$ alloys were confirmed by EDX (Table 1). The alloys were ground into coarse particles and sealed under vacuum in separate quartz tubes with elemental sulfur. In a typical synthesis, we used 300-400 mg of a $Zr_{1-x}Ti_x$ alloy and a calculated amount of sulfur for obtaining stoichiometric $Zr_{1-x}Ti_xS_3$ solid solutions. For the synthesis of TiS₃ and ZrS₃ crystals, we also prepared similar quartz tubes, in

which sulfur was sealed with Ti and Zr powders, respectively. Synthesis of TiS₃ crystals was performed at 500 °C [14], while ZrS₃ crystals were prepared at 800 °C.

Table 1. Chemical composition of the precursor Zr-Ti alloys and the $Zr_{1-x}Ti_xS_3$ needle-like crystals, as determined by EDX.

	EDX results	
Nominal composition of Zr- Ti alloys	Composition of Zr-Ti alloys	Composition of Zr _{1-x} Ti _x S ₃ needle-like crystals
Zr _{0.2} Ti _{0.8}	Zr _{0.21} Ti _{0.79}	$Zr_{0.81}Ti_{0.19}S_{2.81}$
Zr _{0.4} Ti _{0.6}	Zr _{0.42} Ti _{0.58}	Zr _{0.82} Ti _{0.18} S _{2.86}
Zr _{0.6} Ti _{0.4}	Zr _{0.6} Ti _{0.4}	$Zr_{0.83}Ti_{0.17}S_{2.87}$
Zr _{0.8} Ti _{0.2}	Zr _{0.79} Ti _{0.21}	Zr _{0.85} Ti _{0.15} S _{2.92}

The synthesis of $Zr_{1-x}Ti_xS_3$ crystals is illustrated by the scheme in Figure 1b, which shows an ampule with a $Zr_{1-x}Ti_x$ alloy and sulfur. Ampules were annealed in a tube furnace (Lindberg Blue M) at 800 °C for 72 h. After the synthesis, one end of an ampule was moved to a cooler side of a furnace to allow condensation of the excess of sulfur. Needle-like crystals with metallic luster were found on the opposite side of an ampule. The crystals were stored under argon.

SEM images of the samples were collected using a Tescan Vega 3 scanning electron microscope equipped with an Oxford Instruments Aztec EDX system. XRD was performed using a Difray 401 instrument with Cr Kα radiation. Crystallographic analysis of the XRD data was performed using le Bail profile fitting in JANA2006 program [26]. Raman spectra were acquired using a Thermo Scientific DXR Raman microscope with a 532 nm excitation laser. XPS was performed using a Thermo Scientific K-Alpha X-ray photoelectron spectrometer.

For the device fabrication, the Zr_{1-x}Ti_xS₃ crystals were exfoliated using an adhesive tape onto heavily p-doped Si substrates covered with a 300 nm thick layer of SiO₂. Two-terminal devices, in which the exfoliated Zr_{1-x}Ti_xS₃ crystals bridged Cr/Au (3 nm/12 nm) electrodes, were fabricated by standard electron-beam lithography using a Zeiss Supra 40 field-emission scanning electron microscope and a Raith pattern generator. The electron beam deposition of Cr/Au contacts was performed using an AJA electron beam evaporation system. The detailed procedure that we used for the device fabrication can be found in ref. [14]. The devices were imaged by SEM and atomic force microscopy (AFM), which was performed using a Digital Instruments Nanoscope IIIa Dimension 3100 system.

The electrical measurements of $Zr_{1-x}Ti_xS_3$ devices were performed using an Agilent 4155C semiconductor parameter analyzer. The measurements were performed in a Lake Shore TTPX cryogenic probe station at the base pressure of about 2×10^{-6} Torr. The devices were evacuated for at least 2 days before the measurements to minimize the effect of surface adsorbates [27].

3. Results and Discussion

Figure 1c,d shows SEM images of the needle-like crystals that formed at 800 °C in an ampule containing sulfur and the $Zr_{0.6}Ti_{0.4}$ alloy; similar crystals formed from alloys with other compositions. Due to their quasi-1D structure, TiS_3 and ZrS_3 crystals grow in a form of whiskers [3], and similar shape is also expected for the $Zr_{1-x}Ti_xS_3$ solid solutions. We analyzed the composition of the $Zr_{1-x}Ti_xS_3$ needle-like crystals by EDX and found that their Zr:Ti molar ratios were higher than in the precursor alloys (Table 1). Also, while in the Ti-Zr alloys that we prepared the Zr:Ti molar ratios varied in the wide range from 80/20 to 20/80, the resulting needle-like crystals showed little dependence on the alloy composition and contained ~80 at.% of Zr and ~20

at.% of Ti (Table 1). This result agrees well with previous reports on $Zr_{1-x}Ti_xS_3$ solid solutions (0 $\leq x \leq 0.33$), which were grown at 800 °C by chemical vapor transport method from mixtures of sulfur, titanium and zirconium powders [22-24]. The Zr:Ti ratios in the resulting $Zr_{1-x}Ti_xS_3$ crystals were also reported to be higher than in the precursor mixtures [22]. For example, $Zr_{0.66}Ti_{0.33}S_3$ crystals were grown at 800 °C from a precursor mixture with a stoichiometric composition of $Zr_{0.3}Ti_{0.7}S_3$ [22].

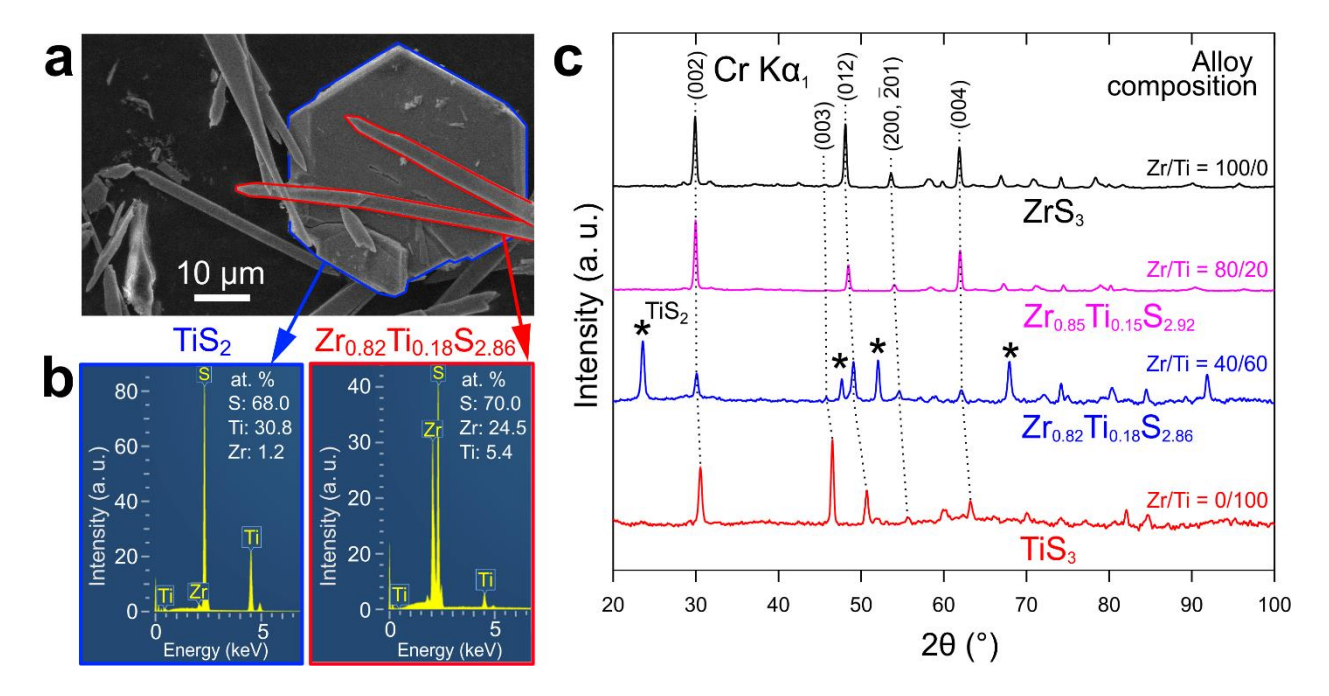


Figure 2. (a) SEM image of the sample grown from the Zr_{0.4}Ti_{0.6} alloy, which shows co-existence of hexagonal (blue outline) and needle-like (red outline) crystals. (b) EDX spectra showing that the hexagonal and needle-like crystals in panel (a) have different compositions. The needle-like crystals have a composition of Zr_{0.82}Ti_{0.18}S_{2.86}, while hexagonal crystals have a composition close to TiS₂. (c) XRD spectra of ZrS₃ (black), TiS₃ (red) and the reaction products synthesized from the Zr_{0.8}Ti_{0.2} (magenta) and Zr_{0.4}Ti_{0.6} alloys (blue). The peaks in the XRD spectra correspond to ZrS₃ (black), Zr_{0.85}Ti_{0.15}S_{2.92} (magenta), Zr_{0.82}Ti_{0.18}S_{2.86} (blue) and TiS₃ (red); the blue spectrum also

contains peaks of the TiS_2 phase, which are indicated by the star symbols. The dotted lines indicate most intense peaks for ZrS_3 , TiS_3 and $Zr_{1-x}Ti_xS_3$ solid solutions.

Figure 2a shows SEM of the products of the reaction between sulfur and the $Zr_{0.4}Ti_{0.6}$ alloy at 800 °C, demonstrating crystals with distinctly different shapes: needles and hexagons. According to the EDX analysis (Figure 2b), the needle-shape crystals had a high zirconium content and an overall composition of $Zr_{0.82}Ti_{0.18}S_{2.86}$ (Table 1); the crystals' shape was consistent with the quasi-1D structure of TMTCs. On the contrary, there was almost no zirconium in the hexagonal crystals, whose composition was close to TiS_2 , a layered material with a hexagonal close packed structure that crystallizes in the $P\overline{3}m1$ space group [28]. EDX data in Table 1 show that the highest measured titanium content was in the needle-like $Zr_{0.81}Ti_{0.19}S_{2.81}$ crystals, which were synthesized from the $Zr_{0.2}Ti_{0.8}$ alloy. Other needle-like $Zr_{1-x}Ti_xS_3$ crystals produced from other alloys had even lower Ti content.

XRD provides further evidence for the formation of the TiS₂ phase in reactions involving Zr-Ti alloys with high Ti content (Figure 2c). According to the EDX results, in case of the Zr_{0.8}Ti_{0.2} alloy the resulting needle-like crystals have a Zr_{0.85}Ti_{0.15}S_{2.92} composition with a comparable Zr:Ti ratio (Table 1) and no hexagonal crystals were observed by SEM. Figure 2c shows that the XRD spectrum of the crystals produced from Zr_{0.8}Ti_{0.2} has a very similar structure to the reference XRD spectrum of ZrS₃. The peaks in the XRD spectrum of Zr_{0.85}Ti_{0.15}S_{2.92} are slightly shifted to larger 2θ angles compared to the peaks in ZrS₃, which occurs due to the smaller size of Ti compared to Zr. This shift corresponds to the decrease in the lattice parameters of Zr_{0.85}Ti_{0.15}S_{2.92} (a = 0.5118 nm, b = 0.3599 nm, c = 0.8989 nm and $\beta = 97.58^{\circ}$) compared to pure ZrS₃ (a = 0.5134 nm, b = 0.3636 nm, c = 0.9003 nm and $\beta = 97.49^{\circ}$). The most considerable relative change is observed for the b parameter (~1.0 %) followed by the changes in a (~0.3 %) and c (~0.2 %) parameters, which

means that the substitution of Zr by Ti in the ZrS₃ structure affects the periodicity along the 1D chains more than their cross-section.

In case of Zr-Ti with larger Ti content, the XRD spectra of reaction products contained TiS_2 peaks, which is illustrated in Figure 2c by the representative spectrum of the crystals prepared from the $Zr_{0.4}Ti_{0.6}$ alloy. Interestingly, the positions of the $Zr_{1-x}Ti_xS_3$ solid solution peaks in this spectrum are nearly the same as $Zr_{0.85}Ti_{0.15}S_{2.92}$ prepared from the $Zr_{0.8}Ti_{0.2}$ alloy, indicating that these solid solutions have comparable compositions, as was also shown by EDX (Table 1). Thus, an increase of the Ti content in the precursor alloy relative to $Zr_{0.8}Ti_{0.2}$ does not translate into a comparable increase of the Ti content in $Zr_{1-x}Ti_xS_3$ solid solution crystals but results in the formation of the secondary TiS_2 phase.

In summary, the XRD, SEM and EDX data demonstrate that in case of the Zr_{0.8}Ti_{0.2} alloy the resulting crystals have a needle-like shape and a Zr_{0.85}Ti_{0.15}S_{2.92} composition with the Zr:Ti molar ratio similar to that in the precursor alloy. We did not observe hexagonal crystals in the reaction product by SEM, and no TiS₂ peaks were detected in the corresponding powder XRD spectrum (Figure 2c). Needle-like crystals could also be grown from the alloys with higher Ti content, but their composition was comparable to crystals grown from the Zr_{0.8}Ti_{0.2} alloy (Table 1). The excessive Ti produced the secondary TiS₂ phase, which was detected by XRD (Figure 2c) and observed in SEM images in the form of hexagonal crystals (Figure 2a). Overall, the formation of the secondary TiS₂ phase is consistent with the large difference in thermal stabilities of TiS₃ and ZrS₃ – according to the S-Ti phase diagram, TiS₃ is only stable below 632 °C and at higher temperatures it should decompose into TiS₂ and S [29], while ZrS₃ is stable above 900 °C [22].

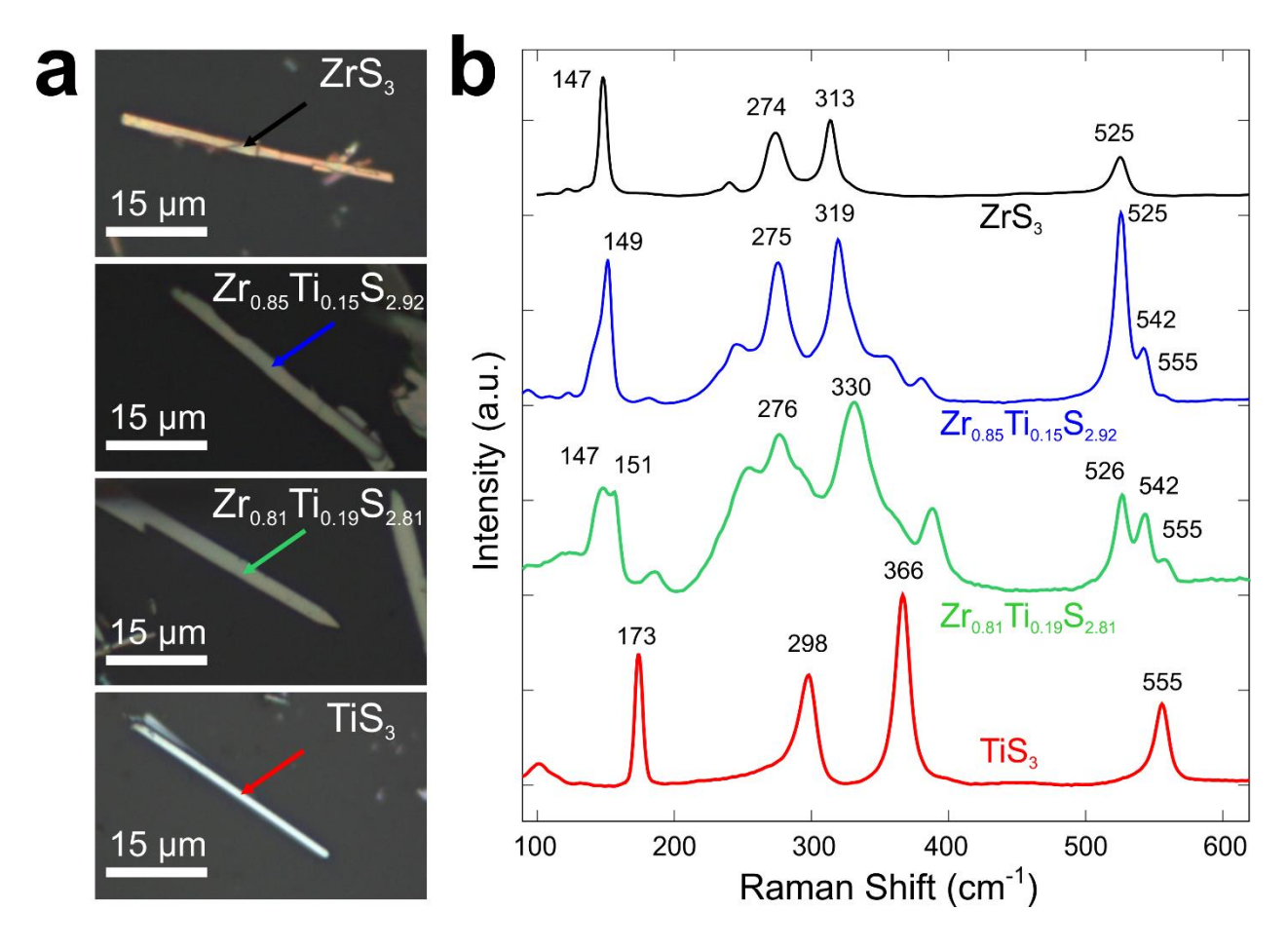


Figure 3. (a) Optical photographs and (b) Raman spectra of ZrS₃, Zr_{0.85}Ti_{0.15}S_{2.92}, Zr_{0.81}Ti_{0.19}S_{2.81} and TiS₃ crystals.

Figure 3 shows optical photographs and Raman spectra of ZrS₃ and TiS₃ crystals, as well the Zr_{0.85}Ti_{0.15}S_{2.92} and Zr_{0.81}Ti_{0.19}S_{2.81} solid solutions with the highest and lowest Zr/Ti ratios prepared in this study. Considering the higher Zr content compared to Ti in the prepared Zr_{1-x}Ti_xS₃ solid solutions, the Raman spectra of Zr_{0.85}Ti_{0.15}S_{2.92} and Zr_{0.81}Ti_{0.19}S_{2.81} are visibly more similar to that of ZrS₃ [30] than TiS₃ [11, 31] (Figure 3b). However, with the substitution of Zr with lighter Ti in the ZrS₃ structure the Raman peaks of ZrS₃ exhibit splittings and shifts to larger wavenumbers. This could be illustrated by the behavior or the 147 cm⁻¹ mode in the Raman spectrum of ZrS₃, which corresponds to out-of-phase rigid vibrations of entire quasi-1D chains in

the opposite directions along the *c* axis (Figure 1a) [11, 30, 31]. With the Ti doping of ZrS₃, this mode gains an additional component at a higher wavenumber (Figure 3b). A similar effect can also be seen for the 525 cm⁻¹ mode of ZrS₃ corresponding to the S-S diatomic vibrations [11, 30, 31], which upon the introduction of Ti in the ZrS₃ structure gains additional components 542 and 555 cm⁻¹. Similar effect was reported previously and identified as the three-mode behavior of the diatomic (S-S)²⁻ vibrations [24].

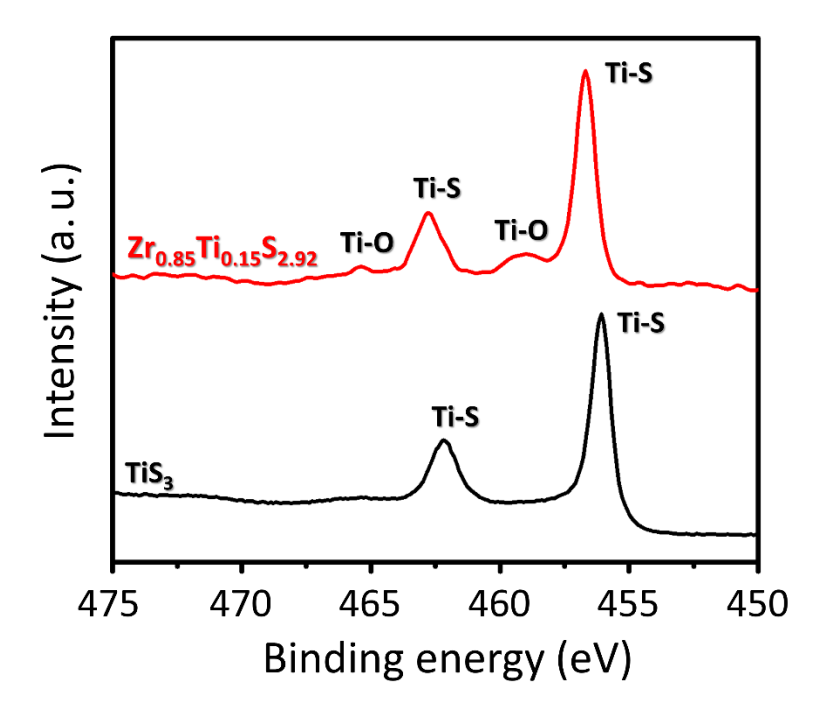


Figure 4. XPS Ti2p spectra of pure TiS₃ and Zr_{0.85}Ti_{0.15}S_{2.92} crystals produced from the Zr_{0.8}Ti_{0.2} alloy.

Since the $Zr_{1-x}Ti_xS_3$ solid solutions produced by the described approach have much higher Zr content compared to Ti, they could be viewed as Ti-doped ZrS_3 . Some information about the coordination of Ti in these solid solutions could be obtained by XPS. Figure 4 shows XPS Ti2p spectra of $Zr_{0.85}Ti_{0.15}S_{2.92}$ crystals produced from $Zr_{0.8}Ti_{0.2}$ alloy, as well as the pure TiS_3 crystals

presented as a reference. The XPS Ti2*p* spectrum of TiS₃ consists of two Ti⁴⁺(2*p*_{1/2}) and Ti⁴⁺(2*p*_{3/2}) components with the binding energies of 462.14 and 456.08 eV, respectively. In this measurement, the XPS was recorded from a freshly cleaved surface of a macroscopically large TiS₃ crystal, so the spectrum did not contain any TiO_x peaks corresponding to the surface oxidation of TiS₃ in air [32]. Such additional peaks at 465.9 and 459.1 eV, which are most likely related to the surface TiO_x [32], were present in the XPS Ti2*p* spectrum of the Zr_{0.85}Ti_{0.15}S_{2.92} crystals, which were measured in the as-prepared form. Most importantly, the major peaks at 462.6 and 456.6 eV, while upshifted in energy, show similar structure to the peaks in the reference XPS Ti2*p* spectrum of TiS₃, suggesting that Ti atoms in the Zr_{0.85}Ti_{0.15}S_{2.92} solid solutions have similar positions in the centers of trigonal sulfur prisms in quasi-1D chains, as in TiS₃ [11]. This conclusion is consistent with the XRD spectrum of Zr_{0.85}Ti_{0.15}S_{2.92}, which shows the same overall pattern as in ZrS₃, although with slightly smaller lattice parameters, which indicates substitution of Zr by Ti in the quasi-1D chains rather than incorporation of Ti in different crystallographic positions and thus change in the crystal structure.

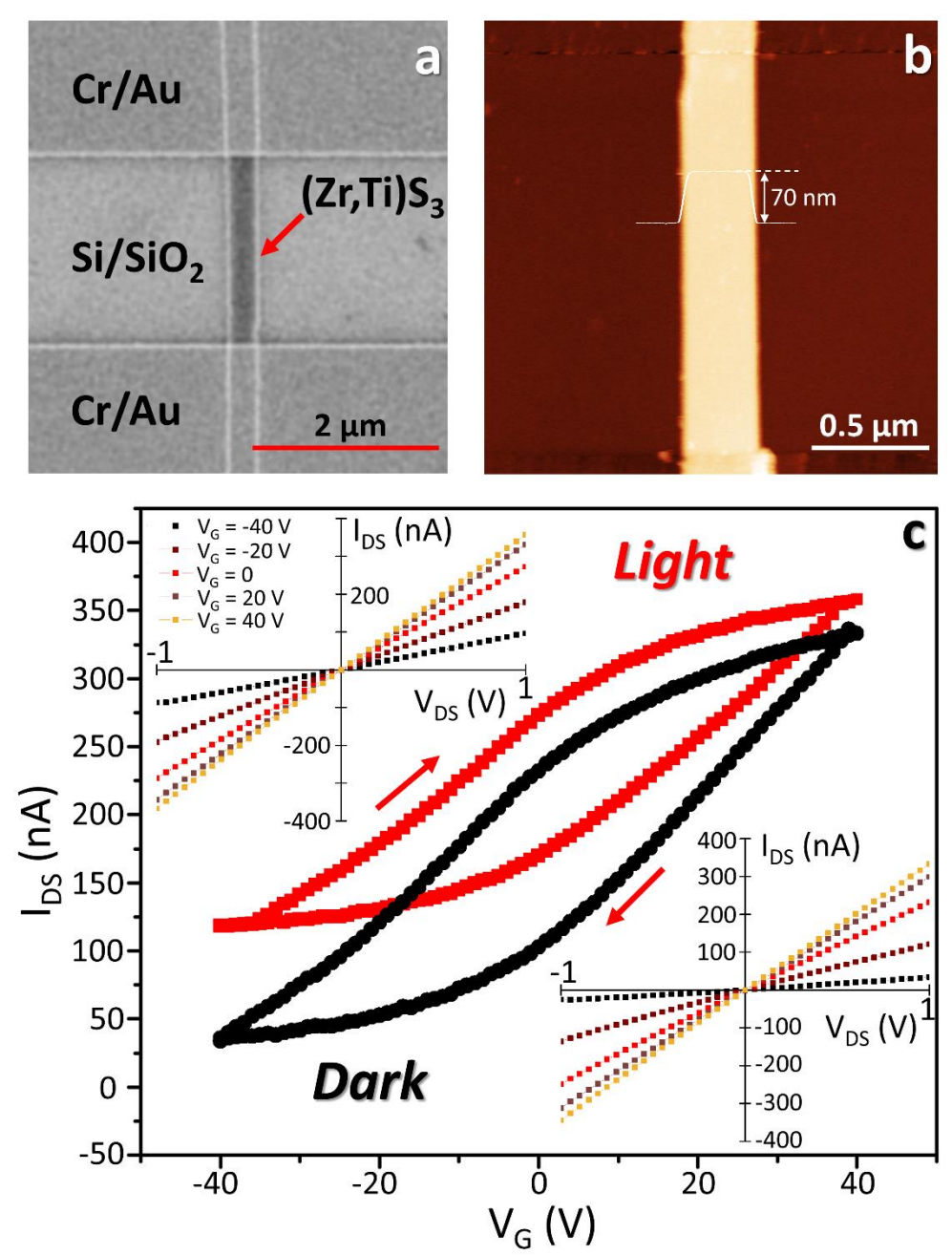


Figure 5. Electrical measurements of the exfoliated $Zr_{1-x}Ti_xS_3$ crystals. (a) SEM and (b) AFM images of a $Zr_{0.82}Ti_{0.18}S_{2.86}$ device. A height profile across the $Zr_{0.82}Ti_{0.18}S_{2.86}$ device channel is overlaid over the panel (b). (c) $I_{DS}-V_G$ dependencies ($V_{DS}=1V$) measured for the device shown in panel (a) in dark (black) and under the visible light illumination (red). The insets show $I_{DS}-V_{DS}$ dependencies measured for the same device in dark (bottom inset) and under the light illumination (top inset) at the gate voltages ranging from -40 to 40 V.

Finally, we investigated the possibility of the mechanical exfoliation of the Zr_{1-x}Ti_xS₃ crystals using an adhesive tape, and the utility of the exfoliated flakes for device fabrication and electrical measurements. Since the reactions of sulfur with different Zr-Ti alloys at 800 °C resulted in the needle-like crystals with very similar compositions (Table 1), we investigated only the Zr_{0.82}Ti_{0.18}S_{2.86} crystals produced from the Zr_{0.4}Ti_{0.6} alloy. Figure 5a shows SEM image of a representative FET device, in which an exfoliated Zr_{0.82}Ti_{0.18}S_{2.86} flake bridges two Cr/Au contacts that served as source (S) and drain (D) electrodes in the electrical measurements. The separation between the S and D electrodes was 2 μm. The devices were fabricated on a silicon substrate covered with a 300-nm-thick layer of SiO₂; the heavily doped p-type silicon served as a global back gate (G) electrode. AFM image of the same device shows that this particular Zr_{0.82}Ti_{0.18}S_{2.86} nanoribbon had a thickness of 70 nm.

Figure 5c summarizes the results of electrical measurements of the device shown in Figure 5a,b. The electrical conductivity of the $Zr_{0.82}Ti_{0.18}S_{2.86}$ device increased when it was illuminated with visible light; this photoresponse is consistent with the previously reported study of the TiS_3 FETs [12]. The insets in Figure 5c show drain-source current (I_{DS}) – drain source voltage (V_{DS}) dependencies measured in dark (bottom inset) and under the illumination (top inset) at the gate voltages ranging from -40 to 40 V. The I_{DS} - V_{DS} dependencies are linear and the conductivities increase with V_G , indicating the n-type conductivity of the channel. The drain-source current (I_{DS}) – gate voltage (V_G) dependencies measured both with and without visible light illumination are hysteretic, which is likely related to the charge traps at the $SiO_2/Zr_{0.82}Ti_{0.18}S_{2.86}$ interface [14]. From the linear regions in the I_{DS} - V_G dependencies we estimated the electron mobilities in $Zr_{0.82}Ti_{0.18}S_{2.86}$ ofabout 2 cm² V^{-1} s⁻¹, which is comparable to the results of Hall effect

measurements of $Zr_{1-x}Ti_xS_3$ solid solutions with similar compositions [22]. For example, $Zr_{0.85}Ti_{0.15}S_3$ crystal were reported to have a Hall effect electron mobility of 1.5 cm² V⁻¹ s⁻¹ [22].

4. Conclusions

In summary, we demonstrated that $Zr_{1-x}Ti_xS_3$ solid solutions could be prepared through the direct reaction between Zr-Ti alloys and sulfur vapor at 800 °C. We varied the Zr/Ti atomic ratio in the alloys from 80/20 to 20/80, and found that in all cases the resulting solid solution crystals had a composition close to $Zr_{0.8}Ti_{0.2}S_3$. The excessive titanium, if present, formed the secondary TiS_2 phase, which was detected by XRD and observed in SEM images in the form of hexagonal crystals. The $Zr_{1-x}Ti_xS_3$ solid solutions formed distinct needle-like crystals, whose shape was consistent with the quasi-1D structure of TMTCs. The $Zr_{1-x}Ti_xS_3$ crystals were characterized by SEM, EDX, XPS and Raman spectroscopy. We demonstrated that these crystals could be mechanically exfoliated into thin nanoribbons by an adhesive tape approach and used for device fabrication and electrical measurements. The transport measurements of $Zr_{0.82}Ti_{0.18}S_{2.86}$ devices revealed their n-type conductivity and electron mobility of about 2 cm² V⁻¹ s⁻¹, as well as photoresponse to visible light. Future studies could be focused at establishing conditions for the growth of $Zr_{1-x}Ti_xS_3$ solutions with substantially different Zr/Ti atomic ratios and assessing their electronic properties in device measurements.

5. Acknowledgements

The authors acknowledge the support by the Ministry of Education and Science of the Russian Federation through grant K2-2018-014. The research at UNL was supported by the nCORE, a wholly owned subsidiary of the Semiconductor Research Corporation (SRC), and the

National Science Foundation (NSF) through grant ECCS-1740136 and the Nebraska Materials Research Science and Engineering Center (NSF DMR-1420645). Some experiments were performed at the Nebraska Nanoscale Facility, which is supported by the NSF (ECCS-1542182) and the Nebraska Research Initiative.

References

- [1] S. Furuseth, L. Brattas, A. Kjekshus, On the Crystal Structures of TiS₃, ZrS₃, ZrSe₃, ZrTe₃, HfS₃, and HfSe₃, Acta Chemica Scandinavica A, 29 (1975) 623-631.
- [2] L. Brattas, A. Kjekshus, On the Properties of Compounds with the ZrSe₃ Type Structure, Acta Chem. Scand., 26 (1972) 3441-3449.
- [3] J.O. Island, A.J. Molina-Mendoza, M. Barawi, R. Biele, E. Flores, J.M. Clamagirand, J.R. Ares, C. Sánchez, H.S.J. van der Zant, R. D'Agosta, I.J. Ferrer, A. Castellanos-Gomez, Electronics and optoelectronics of quasi-1D layered transition metal trichalcogenides, 2D Materials, 4 (2017) 022003.
- [4] D.W. Murphy, F.A. Trumbore, Chemistry of TiS₃ and NbSe₃ Cathodes, J. Electrochem. Soc., 123 (1976) 960-964.
- [5] M. Zanini, J.L. Shaw, G.J. Tennenhouse, The Behavior of Na-TiS₂ and Na-TiS₃ as Solid-Solution Electrodes, J. Electrochem. Soc., 128 (1981) 1647-1650.
- [6] A. Hayashi, T. Matsuyama, A. Sakuda, M. Tatsumisago, Amorphous Titanium Sulfide Electrode for All-solid-state Rechargeable Lithium Batteries with High Capacity, Chem. Lett., 41 (2012) 886-888.

- [7] J. Dai, X.C. Zeng, Titanium Trisulfide Monolayer: Theoretical Prediction of a New Direct-Gap Semiconductor with High and Anisotropic Carrier Mobility, Angewandte Chemie International Edition, 54 (2015) 7572-7576.
- [8] J. Kang, H. Sahin, H.D. Ozaydin, R.T. Senger, F.M. Peeters, TiS₃ nanoribbons: Width-independent band gap and strain-tunable electronic properties, Phys. Rev. B, 92 (2015) 075413.
- [9] J. Zhang, X. Liu, Y. Wen, L. Shi, R. Chen, H. Liu, B. Shan, Titanium Trisulfide Monolayer as a Potential Thermoelectric Material: A First-Principles-Based Boltzmann Transport Study, ACS Applied Materials & Interfaces, 9 (2017) 2509-2515.
- [10] N.V. Morozova, I.V. Korobeinikov, K.V. Kurochka, A.N. Titov, S.V. Ovsyannikov, Thermoelectric Properties of Compressed Titanium and Zirconium Trichalcogenides, The Journal of Physical Chemistry C, 122 (2018) 14362-14372.
- [11] A. Lipatov, M.J. Loes, H. Lu, J. Dai, P. Patoka, N.S. Vorobeva, D.S. Muratov, G. Ulrich, B. Kästner, A. Hoehl, G. Ulm, X.C. Zeng, E. Rühl, A. Gruverman, P.A. Dowben, A. Sinitskii, Quasi-1D TiS₃ Nanoribbons: Mechanical Exfoliation and Thickness-Dependent Raman Spectroscopy, ACS Nano, (2018) DOI: 10.1021/acsnano.1028b07703.
- [12] J.O. Island, M. Buscema, M. Barawi, J.M. Clamagirand, J.R. Ares, C. Sánchez, I.J. Ferrer, G.A. Steele, H.S.J. van der Zant, A. Castellanos-Gomez, Ultrahigh Photoresponse of Few-Layer TiS₃ Nanoribbon Transistors, Advanced Optical Materials, 2 (2014) 641-645.
- [13] J.O. Island, M. Barawi, R. Biele, A. Almazán, J.M. Clamagirand, J.R. Ares, C. Sánchez, H.S.J. van der Zant, J.V. Álvarez, R. D'Agosta, I.J. Ferrer, A. Castellanos-Gomez, TiS₃

 Transistors with Tailored Morphology and Electrical Properties, Adv. Mater., 27 (2015) 2595-2601.

- [14] A. Lipatov, P.M. Wilson, M. Shekhirev, J.D. Teeter, R. Netusil, A. Sinitskii, Few-layered titanium trisulfide (TiS₃) field-effect transistors, Nanoscale, 7 (2015) 12291-12296.
- [15] D. Jariwala, V.K. Sangwan, L.J. Lauhon, T.J. Marks, M.C. Hersam, Emerging Device Applications for Semiconducting Two-Dimensional Transition Metal Dichalcogenides, ACS Nano, 8 (2014) 1102-1120.
- [16] Q. Cui, A. Lipatov, J.S. Wilt, M.Z. Bellus, X.C. Zeng, J. Wu, A. Sinitskii, H. Zhao, Time-Resolved Measurements of Photocarrier Dynamics in TiS₃ Nanoribbons, ACS Applied Materials & Interfaces, 8 (2016) 18334-18338.
- [17] H.G. Grimmeiss, A. Rabenau, H. Hahn, P. Ness, Über elektrische und optische Eigenschaften einiger Chalkogenide von Elementen der IV. Nebengruppe, Z. Elektrochem., 65 (1961) 776–783.
- [18] H. Yi, T. Komesu, S. Gilbert, G. Hao, A.J. Yost, A. Lipatov, A. Sinitskii, J. Avila, C. Chen, M.C. Asensio, P.A. Dowben, The band structure of the quasi-one-dimensional layered semiconductor TiS₃(001), Appl. Phys. Lett., 112 (2018) 052102.
- [19] E. Finkman, B. Fisher, Electrical transport measurements in TiS₃, Solid State Commun., 50 (1984) 25-28.
- [20] I.J. Ferrer, J.R. Ares, J.M. Clamagirand, M. Barawi, C. Sánchez, Optical properties of titanium trisulphide (TiS₃) thin films, Thin Solid Films, 535 (2013) 398-401.
- [21] S. Kurita, J.L. Staehli, M. Guzzi, F. Lévy, Optical properties of ZrS₃ and ZrSe₃, Physica B+C, 105 (1981) 169-173.
- [22] K. Sieber, B. Fotouhi, O. Gorochov, Crystal growth, characterization and photoelectrochemical properties of $Zr_{1-x}Ti_xS_3$ (0 < x < .33), Mater. Res. Bull., 18 (1983) 1477-1484.

- [23] P. Gard, F. Cruege, C. Sourisseau, O. Gorochov, Single-crystal micro-Raman studies of ZrS₃, TiS₃ and several Zr_{1-x}Ti_xS₃ compounds (0 \leq x \leq 0.33), Journal of Raman Spectroscopy, 17 (1986) 283-288.
- [24] P. Gard, C. Sourisseau, O. Gorochov, Effect of Metal Substitution in ZrS_3 and TiS_3 Compounds. Electronic, Raman, and Resonance Raman Study of $Zr_{1-x}Ti_xS_3$ Ternary Phases, 0 < x < 1, physica status solidi (b), 144 (1987) 885-901.
- [25] B. Predel, Ti-Zr (Titanium-Zirconium): Datasheet from Landolt-Börnstein Group IV
 Physical Chemistry · Volume 5J: "Pu-Re Zn-Zr". Springer-Verlag Berlin Heidelberg, 1998.
 [26] V. Petříček, M. Dušek, L. Palatinus, Crystallographic Computing System JANA2006:
 General features, Z. Krist.-Cryst. Mater., 229 (2014) 345-352.
- [27] A. Sinitskii, A. Dimiev, D.V. Kosynkin, J.M. Tour, Graphene Nanoribbon Devices
 Produced by Oxidative Unzipping of Carbon Nanotubes, ACS Nano, 4 (2010) 5405-5413.
 [28] R.R. Chianelli, J.C. Scanlon, A.H. Thompson, Structure refinement of stoichiometric TiS₂,
 Mater. Res. Bull., 10 (1975) 1379-1382.
- [29] J.L. Murray, The S-Ti (Sulfur-Titanium) system, Bulletin of Alloy Phase Diagrams, 7 (1986) 156-163.
- [30] K. Osada, S. Bae, M. Tanaka, H. Raebiger, K. Shudo, T. Suzuki, Phonon Properties of Few-Layer Crystals of Quasi-One-Dimensional ZrS₃ and ZrSe₃, The Journal of Physical Chemistry C, 120 (2016) 4653-4659.
- [31] K. Wu, E. Torun, H. Sahin, B. Chen, X. Fan, A. Pant, D. Parsons Wright, T. Aoki, F.M. Peeters, E. Soignard, S. Tongay, Unusual lattice vibration characteristics in whiskers of the pseudo-one-dimensional titanium trisulfide TiS₃, Nat. Commun., 7 (2016) 12952.

[32] D. Gonbeau, C. Guimon, G. Pfister-Guillouzo, A. Levasseur, G. Meunier, R. Dormoy, XPS study of thin films of titanium oxysulfides, Surface Science, 254 (1991) 81-89.